Soft Matter

ROYAL SOCIETY OF CHEMISTRY

PAPER

View Article Online
View Journal | View Issue

Cite this: *Soft Matter*, 2021, **17**, 10376

Tuning cell adhesion on supported lipid bilayers *via* nanoscale geometry

Long Li,†[a] Jie Gao,†[b] Yingfeng Shao,*[a] Fan Song [ac] and Jinglei Hu *[b]

Received 30th September 2021,
Accepted 19th October 2021

DOI: 10.1039/d1sm01407b

rsc.li/soft-matter-journal

The cell-supported lipid bilayer (SLB) adhesion system has been widely used as the model system to study the receptor–ligand interactions that occur at the membrane interface. The ligand-functionalized SLBs are deposited either directly on solids or on polymer cushions. An important question that arises is whether the geometry of the SLB affects the binding of cell adhesion receptors to the ligands. By using a mesoscopic mechanical model and Monte Carlo simulations, we have investigated the adhesion of a fluid membrane to a corrugated or egg-carton shaped SLB. We find that the nanoscale geometry of the SLB strongly affects the receptor–ligand binding. This effect results from the fact that the adhering membrane bends according to the SLB geometry in order for the adhesion receptors to bind ligands. The membrane bending couples with spatial distribution of the receptor–ligand complexes and membrane thermal undulations. Our results demonstrate that cell adhesion to SLBs can be controlled by tuning the nanoscale geometry of the SLB, and may have profound implications for future development of tissue engineering and regenerative medicine.

1 Introduction

Cell adhesion is of fundamental importance in numerous biological processes, including signal transduction, immune responses, cell locomotion, and tissue formation, and is also involved in a range of pathological diseases such as cancer, cardiovascular diseases, and neurodegenerative diseases.[1–7] Research on cell adhesion has been widely carried out in the fields of cell biology, biomedicine, and tissue engineering, and exploring how to control the cell adhesion has been the key to many biomedical and biotechnological applications.[8] The adhesion processes are mediated by the specific binding of receptors and ligand molecules anchored to the two apposite cell membranes. To fully elucidate the molecular interactions at the membrane interfaces, the supported bilayer systems, in which the phospholipid bilayers containing reconstituted ligand proteins deposit onto solid substrates, have been extensively used as experimental cell-surface models because of their easily tunable architecture, fluidity, and functionalization and have allowed us to gain insight into the two-dimensional receptor–ligand binding. For example, Dustin *et al.*[9] demonstrated that lymphocyte function-associated antigen 3 (LFA-3) is a ligand for CD2 and can mediate T lymphocyte adhesion on a supported lipid bilayer (SLB) containing purified LFA-3 from human erythrocytes. Grakoui *et al.*[10] showed that the T cell activation and the transport of the accumulated peptide-major histocompatibility complexes (pMHC) into the central cluster during immunological synapse formation depend on T cell receptor (TCR)-pMHC binding. Manz *et al.*[11] further found that T-cell triggering thresholds are determined by the number of activating pMHC available to individual TCR clusters. Schmid *et al.*[12] studied the size-dependent organization of membrane proteins at an interface between a SLB and a giant unilamellar vesicle (GUV), and found that non-binding protein exclusion can be affected by the binding protein potential due to lateral crowding.

The key quantity to characterizing the receptor–ligand binding is the equilibrium constant $K = [RL]/([R][L])$[13–16] with the area concentrations of receptor–ligand complexes [RL], unbound receptors [R] and unbound ligands [L]. A variety of techniques such as micropipette aspiration,[16,17] flow chamber,[18] atomic force microscopy,[19] and fluorescence spectroscopy[20] have been used to directly measure the two-dimensional binding constant. However, the measured values of K differ by orders of magnitude, depending strongly on the experimental methods.[2,14,21] Further studies reveal that, in contrast to protein binding in solution, the receptor–ligand binding constant is determined not only by their binding

[a] *State Key Laboratory of Nonlinear Mechanics and Beijing Key Laboratory of Engineered Construction and Mechanobiology, Institute of Mechanics, Chinese Academy of Sciences, Beijing, China. E-mail: shaoyf@lnm.imech.ac.cn; Fax: +86-10-8254-3977; Tel: +86-10-8254-4360*

[b] *Kuang Yaming Honors School and Institute for Brain Sciences, Nanjing University, Nanjing, China. E-mail: hujinglei@nju.edu.cn; Fax: +86-25-8968-1298; Tel: +86-25-8968-1298*

[c] *School of Engineering Science, University of Chinese Academy of Sciences, Beijing, China*

† These authors contributed equally to this work.

energy but also by a number of other factors, *e.g.*, protein flexibility,[22] external force,[23] membrane properties[2,24] and organization.[17,25,26] Particularly, utilizing the cell-substrate system in which Jurkat cells constitutively expressing CD2 adhere to CD58-functionalized SLBs, Tolentino *et al.* found a 3–4 orders of magnitude difference in the binding affinities measured by mechanical and fluorescence methods, which is suggested to be attributed to the different number of adhesion proteins in the contact area.[27] Fenz *et al.*[28] identified the membrane fluctuation as a source of long-range *cis*-interactions between cadherin bonds in the adhesion of GUV decorated with E-cadherin to SLB that is also functionalized with E-cadherin, and reported that the membrane fluctuations introduce cooperativity in *trans*-interactions. The experimentally-confirmed cooperative binding, combined with previous theoretical predictions by Krobath *et al.*,[2] helps to explain the significant difference in the measured binding constant. Recent developments in advanced nanotechnology enable researchers to study the role of the physiologically relevant geometry of lipid membranes on a nanoscale in cell adhesion and relevant processes, which is vital for broad applications in cell research, drug discovery, and tissue engineering.[29] A central question that remains is how the nanoscale geometry of SLBs affects the receptor–ligand binding in the cell-SLB adhesion system.

Here, we report Monte Carlo (MC) simulations of a mesoscopic model for cell-SLB adhesion. We consider two smooth SLB profiles: a corrugated profile and an egg-carton profile with height h and width w, as illustrated in Fig. 1. We find that, in the biologically relevant range of model parameters, the binding affinity of receptors and ligands is significantly reduced by the presence of SLB profiles, yielding a decrease of more than one order of magnitude in the binding constant K. The decrease in K can be understood from the conformational entropy and bending energy of the flexible membrane, and translational entropy of adhesion proteins. Meanwhile, we show that the overall contribution made by the three factors to the binding constant can be quantified by the membrane area fraction within the receptor–ligand binding range. Our findings suggest that the SLB geometry on nanoscale proves an effective means for controlling the receptor–ligand binding and cell adhesion.

2 Models and methods

Consider a cell-substrate adhesion system where a cell membrane anchored with receptors adheres to a ligand-functionalized SLB. Cell adhesion involves multiple processes, such as the fluctuation of a flexible membrane, lateral diffusion of protein molecules, and binding and unbinding of receptors and ligands. The length and time scales associated with these processes differ by orders of magnitude. To deal with such complexity, we employ a classic mesoscopic model for the adhesion of membranes *via* receptor–ligand binding.[21,30–32] In this model, both the cell membrane and the supported lipid bilayer are described as two-dimensional elastic surfaces that can be parameterized with respect to a reference horizontal plane of square lattices, as illustrated in Fig. 1. To capture the whole spectrum of bending deformations of the flexible membrane, the size of each quadratic patch on the lattice is chosen to be a = 5 nm.[2,33,34] The configuration of the flexible membrane is specified by the height field $\{z_i\}$ relative to the reference plane at lattice site i. The elastic bending energy of the flexible tensionless membrane is then written in a discretized form as[35,36]

$$\mathscr{H}_{\mathrm{be}} = \frac{\kappa}{2a^2}\sum_i (\Delta_{\mathrm{d}} z_i)^2 \tag{1}$$

where κ is the bending rigidity of the cell membrane, and $\Delta_{\mathrm{d}} z_i$ is the discretized Laplacian of the height field $\{z_i\}$. We choose a typical value of $\kappa = 25 k_{\mathrm{B}}T$ for the bending rigidity.[2] In contrast to the cell membrane, the supported lipid bilayer on the substrate assumes a constant shape and thus a constant bending energy that does not affect the behavior of the adhesion system. We consider two smooth SLB profiles: a corrugated profile (Fig. 1(a)) and an egg-carton profile (Fig. 1(b)) with height h and width w, as described by $z = h\cos(2\pi x/w)$ and $z = h\cos(2\pi x/w)\cos(2\pi y/w)$, respectively. Experimentally, SLBs with such profiles can be prepared by fabricating the substrate with a similar geometry through the use of electron-beam lithography and nanoimprint.[37–40] Here, we consider height h = 0–20 nm and width w = 150–300 nm.

The adhesion receptor and ligand proteins occupy single vacant membrane patches and bind specifically with a 1 : 1

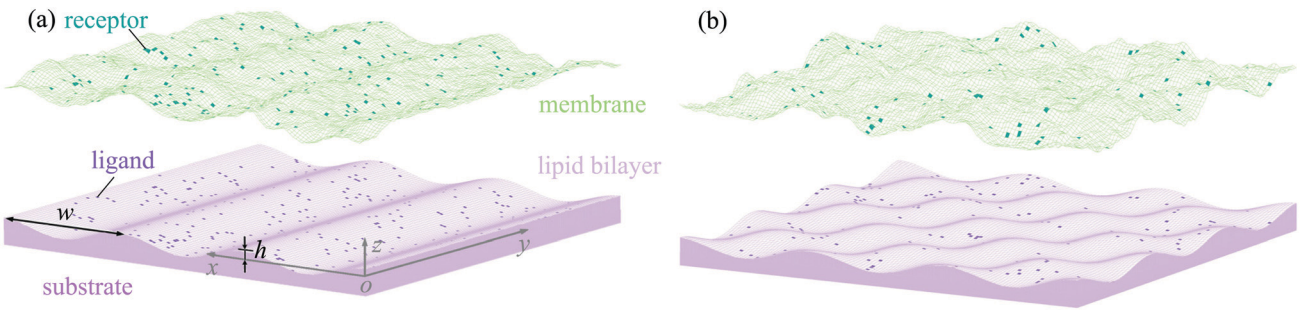

Fig. 1 Snapshots from Monte Carlo simulation of a fluid membrane adhering to a supported lipid bilayer *via* the specific binding of receptors (in green) and ligands (in purple). The supported lipid bilayer assumes a smooth corrugated profile $z(x) = h\cos(2\pi x/w)$ in (a) or egg-carton profile $z(x,y) = h\cos(2\pi x/w)\cos(2\pi y/w)$ in (b) with height h and width w. The model is explained in detail in the main text.

stoichiometry. The spatial distribution of receptors in the upper cell membrane is described by the composition field $\{m_i^+\}$ with values $m_i^+ = 0$ or 1 indicating the absence or presence of receptors at patch i. Likewise, $\{m_i^-\}$ with values $m_i^- = 0$ or 1 describes the spatial distribution of ligands in the lower SLB. A receptor–ligand binding event occurs only when the receptor and ligand molecules are opposite to each other and within the binding range, *i.e.*, $l_c - l_b/2 < l_i < l_c + l_b/2$, where l_c is the length of the receptor–ligand complex, l_b is the width of the square-well binding potential V_b, and l_i is the separation of the two opposite patches at site i. The interaction energy of receptors and ligands within the contact zone is then given by[34,41]

$$\mathscr{H}_{bi} = \sum_i V_b m_i^+ m_i^- = -u_b \sum_i m_i^+ m_i^- \theta\left(\frac{l_b}{2} - |l_i - l_c|\right) \quad (2)$$

where $u_b > 0$ is the binding energy. The Heaviside's step function $\theta(\cdots) = 0$ if the receptor and its binding partner are separated beyond the binding range. Using this treatment, the potential in eqn (2) effectively takes into account the binding specificity by incorporating the distance- and orientation-dependence of the receptor–ligand binding. We choose binding energy $u_b = 6k_BT$, potential range $l_b = 1$ nm, and receptor–ligand complex length $l_c = 15$ nm.[2,34] The area concentration of the receptor and ligand proteins is $c_R = c_L = c_p = 1000\ \mu m^{-2}$.[24]

We perform MC simulations with a standard Metropolis algorithm to study the equilibrium behavior of the adhesion system in a canonical ensemble with an overall configurational energy $\mathscr{H}_{ad} = \mathscr{H}_{be} + \mathscr{H}_{bi}$. Two types of trial moves are used in the simulations: (i) vertical displacement of membrane patches to capture the thermal shape fluctuations of the cell membrane, (ii) lateral translation of the receptors and ligands to mimic their diffusion. In the MC trial moves of type (i), we attempt to shift transversely the height field $\{z_i\}$ for each patch of the upper membrane. To prevent the overlap of the upper cell membrane and lower SLB, all trial moves leading to $l_i < 0$ are rejected. In the MC trial moves of type (ii), each protein molecule is allowed to jump to one of the four nearest-neighbor lattices with equal probability during a single MC step. Considering the different physical time scales of the two motions, we conduct trial moves of type (i) for each lattice site 10 times and trial move of type (ii) for each receptor and ligand molecules once on average in one MC cycle.[26] Both types of local trial moves can lead to possible variations $\Delta\mathscr{H}_{ad}$ in the overall configurational energy by changing the membrane bending energy $\mathscr{H}_{be}$ and receptor–ligand interaction energy $\mathscr{H}_{bi}$. Following the standard Metropolis criterion, a trial move is accepted with the probability $\exp(-\Delta\mathscr{H}_{ad}/k_BT)$.

We have simulated the adhering membrane with 120×120 patches (*i.e.*, 600×600 nm^2) under periodic boundary conditions. In each simulation, we start with a planar cell membrane at a distance of $l_c = 15$ nm from the crest of the lower SLB. The receptors and ligands are initially randomly distributed on the cell membrane and SLB, respectively. A relaxation run of 5×10^7 MC cycles is used for thermal equilibration and a subsequent run of 5×10^7 MC cycles for statistical sampling. The simulation results are an average over 10 independent realizations unless otherwise specified.

3 Results and discussion

Fig. 2 shows the equilibrium constant K of the receptor–ligand binding that mediates the adhesion against the profile height h of the SLB assuming corrugated or egg-carton shapes as obtained from MC simulations. Each data set corresponds to the same type of SLB shape (corrugated in filled circles, egg-carton in empty circles) but different values of profile width w as specified in the legend. The quantity $a^2e^{u_b/k_BT}$ used to rescale K is the receptor–ligand binding constant in the case of a planar membrane without shape fluctuations adhering to a flat SLB. For either type of SLB shape, the binding constant K decreases with increasing h at a fixed w, while it increases with w at a fixed h. It is remarkable that an egg-carton shaped SLB with a profile height $h = 20$ nm and width $w = 150$ or 200 nm leads to about 20-fold decrease in K compared to the case of a flat SLB ($h = 0$). Such a change in K translates to a free energy change of about $3k_BT$ per receptor–ligand bond, indicating that nanoscale geometry can be introduced into the SLB to effectively tune its adhesion with cell membranes. Fig. 2 also shows that at fixed values of profile height h and width w, the binding constant K is larger for corrugated SLBs than for egg-carton SLBs, *i.e.*, the adhesion receptors bind more strongly to ligands mobilized on corrugated SLBs than to those on egg-carton SLBs.

To visualize the effect of SLB geometry on the adhesion, we present in Fig. 3 the simulation snapshots of the adhesion systems at a different profile height h for the SLB. For clarity, only the receptors (green patches) and ligands (purple patches) that are bound to form complexes are displayed in these snapshots. At a small height $h = 5$ nm (left panels), the membrane

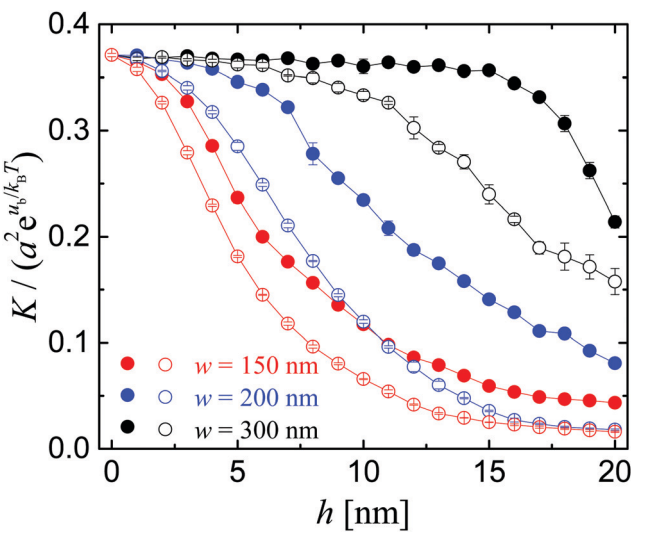

Fig. 2 Rescaled binding constant K as a function of the profile height h for corrugated (filled circle) and egg-carton (empty circle) SLBs with different widths w obtained from MC simulations.

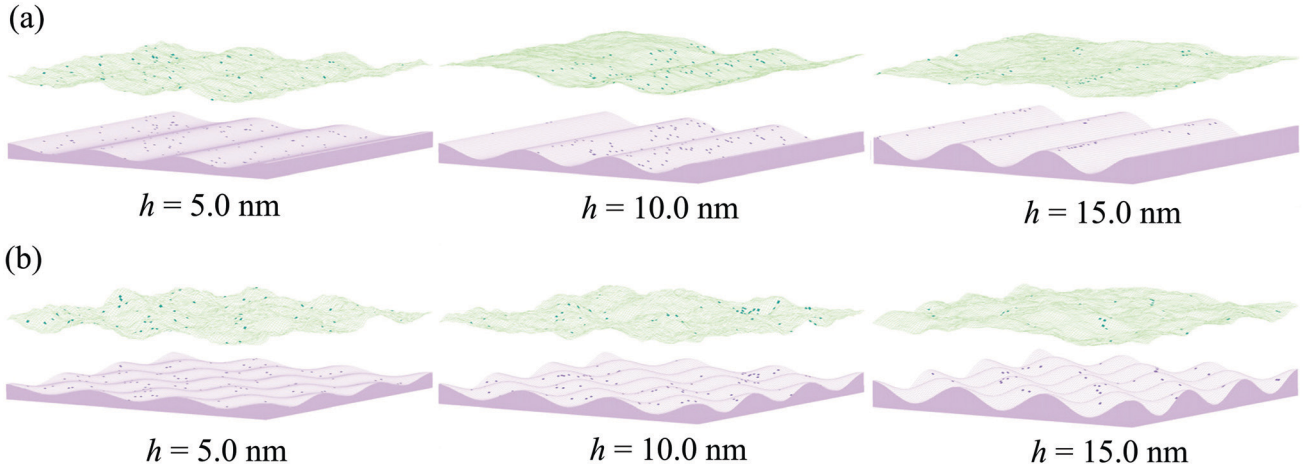

Fig. 3 Simulation snapshots of flexible membranes adhering to corrugated (a) and egg-carton (b) shaped SLBs with profile heights h = 5.0, 10.0 and 15.0 nm at a fixed profile width w = 200 nm. For clarity, only the bound receptors and ligands that form complexes are displayed here. The color code is the same as in Fig. 1, *i.e.*, receptors in green, and ligands in purple.

curves to match the geometry of the SLB in order to form more receptor–ligand bonds which restrict the local membrane-SLB separation, and the bonds are distributed rather uniformly over the membrane interface. At an intermediate height h = 10.0 nm (middle panels), the upper membrane ceases to completely follow the profile of the SLB, and the ligands tend to be situated in the upper part of the corrugated or egg-carton SLB in order to bind the adhesion receptors. At a large height h = 15.0 nm (right panels), the flexible membrane appears to undulate around a flat state regardless of the SLB geometry, and the bound ligands are most likely found in the vicinity of the SLB crests. Fig. 3 illustrates a delicate interplay of membrane bending and receptor–ligand binding that depends on the profile of the SLB.

To understand the role of membrane bending in receptor–ligand binding, we estimate the bending energy of the adhering membrane, E_{be}, from its average shape. The ratio of E_{be} to the bending energy required by the membrane to assume exactly the same shape as the SLB, $E_{be,SLB}$, is then determined to

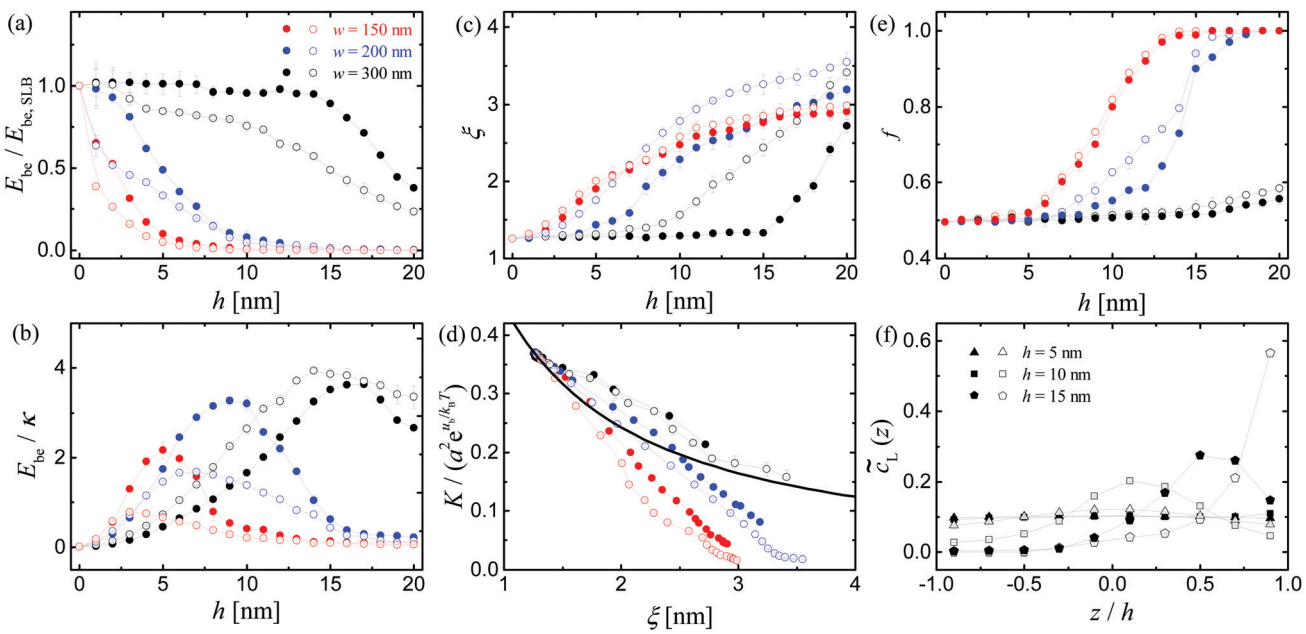

Fig. 4 Membrane bending energy (a and b), thermal roughness (c and d), and spatial distribution of bound ligands (e and f) in response to the SLB geometry. (a and b) Rescaled and absolute bending energy of the adhering membrane against SLB profile height h. E_{be} is the bending energy for the average shape of the adhering membrane, and $E_{be,SLB}$ is the bending energy required by the membrane to assume the same shape as the SLB. (c) Membrane roughness ξ *versus* h. (d) The receptor–ligand binding constant K *versus* ξ. The solid line is given by $K/(a^2 e^{u_b/k_BT}) = [1 + (\xi/\ell)^2]^{-1/2}$ with the length scale ℓ = 0.35 nm obtained from the case of the planar SLB. (e) Percentage f of receptor–ligand complexes with bound ligands residing in the upper half of the SLB. (f) Normalized concentration profile $\tilde{c}_L(z)$ of bound ligands on the SLB for different profile heights h at a fixed profile width w = 200 nm.

understand as to what extent the adhering membrane matches the SLB geometry. Fig. 4(a) shows that the ratio $E_{be}/E_{be,SLB}$ decreases from 1 as the profile height h increases, consistent with our visualization of the snapshots in Fig. 3. For w = 300 nm (black circles), the membrane's average shape is somewhat correlated with the SLB geometry even at a large h; for w = 150 and 200 nm (red and blue circles), the membrane undulates around the flat configuration and does not match the SLB geometry at all at large h. Fig. 4(b) shows that E_{be} first increases and then decreases with h. This change in membrane bending energy cannot explain the monotonic decrease of the binding constant K in Fig. 2, since a decrease in E_{be} would have favored the receptor–ligand binding if there were no other factors affecting the binding. We also quantify the thermal fluctuations of the adhering membrane around its average shape by the membrane roughness $\xi = \left[\sum_{i=1}^{N}\left(\overline{z_i^2} - \overline{z_i}^2\right)\Big/N\right]^{1/2}$. Here, $\overline{z_i^2}$ and $\overline{z_i}$ are averages at membrane site i and the field $\{\overline{z_i}\}$ describes the average shape of the membrane. The larger the ξ, the more the fluctuation modes of the membrane around its average shape, and the larger the membrane conformational entropy. Since the receptor–ligand complex constrains the local separation of the membrane from the SLB, a larger membrane roughness thus corresponds to a smaller K. Fig. 4(c) illustrates that the thermal roughness ξ increases with h, in qualitative agreement with the decrease of K with h in Fig. 2. Note that in the case of the corrugated SLB with w = 300 nm (black filled circles), ξ increases very slightly with h when $h < 15$ nm, while the binding constant K slightly decreases with h. We plot K against ξ in Fig. 4(d) and find that the data points do not collapse to a single curve and each data set shows quantitative discrepancy from the theoretical prediction $K/(a^2e^{u_b/k_BT}) = [1 + (\xi/\ell)^2]^{-1/2}$ that holds for the case of the planar SLB or unsupported, fluctuating lipid bilayer.[24] Fig. 4(d) indicates that in the adhesion system with the corrugated or egg-carton shaped SLB, the thermal roughness of the adhering membrane is not the only physical property that determines the rescaled binding constant $K/(a^2e^{u_b/k_BT})$.

The translational entropy of the receptor–ligand complexes coupled to the average shape of the adhering membrane also affects the receptor–ligand binding. The coupling can be explained by considering two ideal shapes of the adhering membrane. For a flat membrane, the receptor–ligand complexes only form on a fraction of the membrane sites with proper separations from the SLB. For a membrane with the same shape as the SLB, the complexes can form on any membrane site and therefore have larger translational entropy than in the case of a flat membrane. Fig. 4(e) shows the percentage f of receptor–ligand complexes whose bound ligands reside in the upper half of the SLB. f = 0.5 corresponds to the case where the bound ligands have no preference for the lower or upper half of the SLB, and f = 1.0 is the case where the bound ligands are only situated in the upper half. The receptor and ligand molecules will lose more translational entropy upon binding in the latter case than in the former case. f slightly increases with h for the SLB profile width w = 300 nm, in contrast to the systems with w = 150 or 200 nm. The increase of f with h in Fig. 4(e) and the decrease of $E_{be}/E_{be,SLB}$ with h in Fig. 4(a) seem to suggest that the SLB with a larger h causes more translational entropy loss of the complexes and therefore leads to smaller binding constant K. The translational entropy argument is supported by the spatial distribution of bound ligands over the SLB surface as shown in Fig. 4(f). Here, we divide the SLB surface along the z-direction into 10 equal segments and compute the area concentration of bound ligands in each segment, $c_L(z)$, which is then normalized to give the concentration profile $\tilde{c}_L(z) = c_L(z)\Big/\sum_{z=-h}^{+h} c_L(z)$. Fig. 4(f) shows that for a given SLB profile width w, the bound ligands are uniformly distributed in each segment at small h and prefer to reside in the vicinity of the SLB crest as h increases. Fig. 4(e) and (f) imply that the translational entropy of the receptor–ligand complexes depends on the SLB profile.

Our analysis in Fig. 4 reveals that the conformational entropy and curvature energy of the membrane as well as the translational entropy of the proteins are coupled in a SLB-profile-dependent fashion. It is interesting to see whether their overall effect on the receptor–ligand binding constant K can be quantified by the area fraction P_b of the membrane within the binding range of the receptors and ligands. Previous studies have shown that $K/(a^2e^{u_b/k_BT}) = P_b$ for systems with a flexible membrane adhering to another flexible or supported flat membrane.[2,34] For our adhesion systems with corrugated and egg-carton shaped SLBs, Fig. 5 shows that the simulation data are well fitted to $K/(a^2e^{u_b/k_BT}) = P_b$, indicating that the relationship between binding constant K and area fraction P_b generally holds, independent of the SLB geometry. Further theoretical investigation needs to be carried out to calculate the entropic and energetic contributions to the binding free energy.

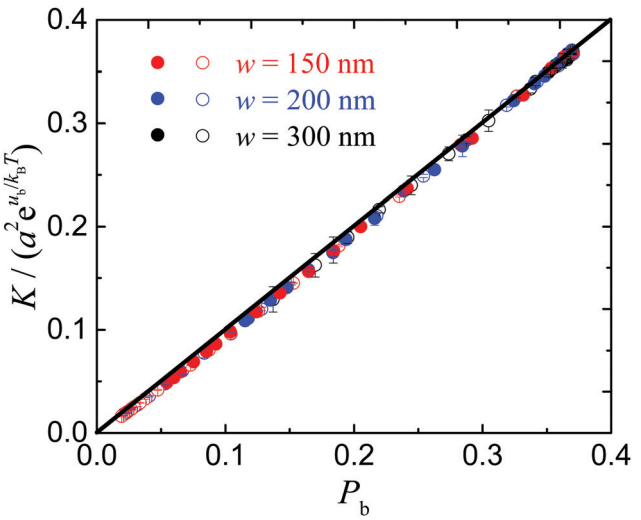

Fig. 5 Receptor–ligand binding constant K as a function of area fraction P_b of the membrane sites that lies within the binding range of the receptors and ligands. The line is given by $K/(a^2e^{u_b/k_BT}) = P_b$. The data points are from the same MC simulations as before.

4 Conclusions

We have investigated the impact of nanoscale geometry of SLBs on the binding of membrane-anchored receptors to ligands grafted on a SLB by means of MC simulations based on a classical statistical mechanical model. Here, we consider corrugated and egg-carton SLB profiles with different height h and width w. In the biologically relevant range of model parameters, we find that the nanoscale geometry of the SLB strongly affects the receptor–ligand binding, depending on the profile of the SLB. More specifically, our results show that for either type of SLB shape, the binding constant K decreases with an increasing h at a fixed w, while increases with w at fixed h. It is remarkable that an egg-carton shaped SLB with profile height h = 20 nm and width w = 150 or 200 nm leads to about 20-fold decrease in K. The comparison of the results for corrugated and egg-carton SLB profiles with the same height and width reveals that the decrease of the binding constant is more pronounced in the latter case. These effects are attributed to the fact that the adhering membrane bends according to the SLB geometry in order for the cell adhesion receptors to bind ligands mobilized on the SLB, accompanied by the change of spatial distribution of the receptor–ligand complexes and membrane thermal undulations. It further reveals that the curvature energy and conformational entropy of the membrane as well as the translational entropy of the adhesion proteins are coupled to affect the binding constant K in a SLB-profile-dependent fashion, and their overall effect on K can be quantitatively determined by measuring the area fraction P_b of the flexible membrane within the binding range of the receptors and ligands, irrespective of whether the SLB is planar or not. Meanwhile, it is found that the thermal roughness of the adhering membrane is not the only physical property that determines the rescaled binding constant for corrugated and egg-carton SLB profiles, in contrast to the case of planar SLB or unsupported, fluctuating lipid bilayers. Theoretically, the respective contribution of curvature energy and conformational entropy of the membrane as well as the translational entropy of the adhesion proteins to the receptor–ligand binding needs to be quantified in further studies.

In practice, the lipid bilayer can be deposited onto the substrate directly or placed on the substrate using lipopolymer tethers. Recent developments in advanced nanoscale technologies make it possible to create a SLB of virtually any geometry by controlling the substrate topology, and allow more precise quantitative experimentation for investigating the fundamental mechanisms of cell adhesion *in vitro*. Here, we report a statistical model to study the cell-SLB adhesion system with a smooth SLB profile, which can be obtained by engineering the substrate topography at nanoscale through the use of, *e.g.*, electron-beam lithography and nanoimprint. This methodology can be extended to deal with other SLB geometries, and the general mechanisms for hindered receptor–ligand binding uncovered here should also exist. Overall, our work offers a more feasible way to control cell adhesion in practical applications due to the easily tunable geometry of SLBs, as compared with other complex methods such as the inhibition of adhesion protein gene expression, and can provide some reference and guide for future development of tissue engineering and regenerative medicine. Moreover, the geometry-regulated receptor–ligand binding we report here may have already been utilized in cellular systems, since the actin cytoskeleton attached to the cell membrane can actively change the nanoscale geometry of the membrane.

Author contributions

J. H. and Y. S. designed the research project; L. L. and J. G. performed computer simulations; J. H. supervised the computer simulations; L. L., J. H., Y. S. and F. S. analyzed and interpreted the results; L. L. and J. H. wrote the manuscript.

Conflicts of interest

There are no conflicts to declare.

Acknowledgements

L. Li, J. Hu and F. Song acknowledge support from the National Natural Science Foundation of China (Grants No. 11902327, 11972041, 21973040 and 21504038), Youth Innovation Promotion Association CAS, and the Strategic Priority Research Program of the Chinese Academy of Sciences (Grant No. XDB22040102). The numerical calculations have been performed using the computing facilities in the High Performance Computing Center (HPCC) of Nanjing University.

Notes and references

1 T. R. Weikl and R. Lipowsky, *Biophys. J.*, 2004, **87**, 3665–3678.
2 H. Krobath, B. Różycki, R. Lipowsky and T. R. Weikl, *Soft Matter*, 2009, **5**, 3354–3361.
3 P. A. van der Merwe and O. Dushek, *Nat. Rev. Immunol.*, 2011, **11**, 47–55.
4 B. W. Benham-Pyle, B. L. Pruitt and W. J. Nelson, *Science*, 2015, **348**, 1024–1027.
5 L. Li and F. Song, *Natl. Sci. Rev.*, 2020, **7**, 1277–1279.
6 L. Li, X. H. Wang, H. L. Wu, Y. F. Shao, H. P. Wu and F. Song, *Front. Mol. Biosci.*, 2021, **8**, 655662.
7 P. Romani, L. Valcarcel-Jimenez, C. Frezza and S. Dupont, *Nat. Rev. Mol. Cell Bio.*, 2021, **22**, 22–38.
8 S. Cai, C. Wu, W. Yang, W. Liang, H. Yu and L. Liu, *Nanotechnol. Rev.*, 2020, **9**, 971–989.
9 M. L. Dustin, M. E. Sanders, S. Shaw and T. A. Springer, *J. Exp. Med.*, 1987, **165**, 677–692.
10 A. Grakoui, S. K. Bromley, C. Sumen, M. M. Davis, A. S. Shaw, P. M. Allen and M. L. Dustin, *Science*, 1999, **285**, 221–227.
11 B. N. Manz, B. L. Jackson, R. S. Petit, M. L. Dustin and J. Groves, *Proc. Natl. Acad. Sci. U. S. A.*, 2011, **108**, 9089–9094.

12 E. M. Schmid, M. H. Bakalar, K. Choudhuri, J. Weichsel, H. S. Ann, P. L. Geissler, M. L. Dustin and D. A. Fletcher, *Nat. Phys.*, 2016, **12**, 704–711.
13 G. I. Bell, *Science*, 1978, **200**, 618–627.
14 M. L. Dustin, S. K. Bromley, M. M. Davis and C. Zhu, *Annu. Rev. Cell Dev. Biol.*, 2001, **17**, 133–157.
15 J. Steinkühler, B. Różycki, C. Alvey, R. Lipowsky, T. R. Weikl, R. Dimova and D. E. Discher, *J. Cell Sci.*, 2019, **132**, jcs216770.
16 C. Zhu, W. Chen, J. Z. Lou, W. Rittase and K. T. Li, *Nat. Immunol.*, 2019, **20**, 1269–1278.
17 J. Huang, V. I. Zarnitsyna, B. Liu, L. J. Edwards, B. D. Jiang, N. Evavold and C. Zhu, *Nature*, 2010, **464**, 932–936.
18 L. Limozin, P. Bongrand and P. Robert, *Sci. Rep.*, 2016, **6**, 35193.
19 T. L. L. Doan, Y. Guerardel, P. Loubiere, M. Mercier-Bonin and E. Dague, *Biophys. J.*, 2011, **101**, 2843–2853.
20 G. P. O'Donoghue, R. M. Pielak, A. A. Smoligovets, J. J. Lin and J. T. Groves, *eLife*, 2013, **2**, e00778.
21 T. R. Weikl, J. L. Hu, G. K. Xu and R. Lipowsky, *Cell Adhes. Migr.*, 2016, **10**, 576–589.
22 N. W. Moore and T. L. Kuhl, *Biophys. J.*, 2006, **91**, 1675–1687.
23 A. S. Smith, K. Sengupta, S. Goennenwein, U. Seifert and E. Sackmann, *Proc. Natl. Acad. Sci. U. S. A.*, 2008, **105**, 6906–6911.
24 J. Hu, R. Lipowsky and T. R. Weikl, *Proc. Natl. Acad. Sci. U. S. A.*, 2013, **110**, 15283–15288.
25 H. A. Anderson and P. A. Roche, *BBA-Mol. Cell Res*, 2015, **1853**, 775–780.
26 L. Li, J. Hu, X. H. Shi, Y. F. Shao and F. Song, *Soft Matter*, 2017, **13**, 4294–4304.
27 T. P. Tolentino, J. Wu, V. I. Zarnitsyna, Y. Fang, M. L. Dustin and C. Zhu, *Biophys. J.*, 2008, **95**, 920–930.
28 S. F. Fenz, T. Bihr, D. Schmidt, R. Merkel, U. Seifert, K. Sengupta and A. S. Smith, *Nat. Phys.*, 2017, **13**, 906–913.
29 S. Cai, C. Wu, W. Yang, W. Liang, H. Yu and L. Liu, *Nanotechnol. Rev.*, 2020, **9**, 971–989.
30 L. Li, Y. Shao, W. Li and F. Song, *Sci. China: Phys. Mech. Astron.*, 2018, **61**, 128711.
31 A. H. Bahrami and T. R. Weikl, *Nano Lett.*, 2018, **18**, 1259–1263.
32 M. Knezevic, H. D. Jiang and S. S. Wang, *Nano Lett.*, 2018, **121**, 238101.
33 R. Goetz, G. Gompper and R. Lipowsky, *Phys. Rev. Lett.*, 1999, **82**, 221–224.
34 B. Różycki, R. Lipowsky and T. R. Weikl, *New J. Phys*, 2010, **12**, 095003.
35 L. Li, J. Hu, B. Różycki and F. Song, *Nano Lett.*, 2020, **20**, 722–728.
36 L. Li, J. Hu, G. Xu and F. Song, *Phys. Rev. E*, 2018, **97**, 012405.
37 S. Bandyopadhyay, A. E. Miller, H. C. Chang, G. Banerjee, V. Yuzhakov, D.-F. Yue, R. E. Ricker, S. Jones, J. A. Eastman, E. Baugher and M. Chandrasekhar, *Nanotechnology*, 1996, **7**, 360–371.
38 J. Feng and T. Okamoto, *Opt. Lett.*, 2005, **30**, 2302–2304.
39 M. Häffner, A. Heeren, M. Fleischer, D. P. Kern, G. Schmidt and L. W. Molenkamp, *Microelectron. Eng.*, 2007, **84**, 937–939.
40 J. Y. Chen and K. W. Sun, *Sol. Energy. Mater. Sol. C*, 2010, **94**, 629–633.
41 L. Li, J. L. Hu, H. P. Wu and F. Song, *Sci. China: Phys. Mech. Astron.*, 2021, **64**, 108712.

